Experimental study and application of computational fluid dynamics on the prediction of air velocity and temperature in a ventilated chamber

M. S. Sharifi, M. Mahdi[*] and K. Maghsoudi

Department of Mechanical Engineering, Shahid Rajaee Teacher Training University, Tehran, Iran.

Abstract

The shape of air flow in the interior is heavily influenced by the air distribution system and the way air enters and exits. By numerically simulating flow through computational fluid dynamics, one can determine the flow pattern and temperature distribution and with the help of the results, provide an optimal design of the air conditioning system. In this study, a chamber is first constructed, and the temperature distribution inside it is measured. There is a fan installed at the back of the chamber for drainage. At the chamber entrance, three inlets for entering the flow are considered. The air entering from the middle inlet is heated by a heater. To prevent heat loss, the body of the enclosure is insulated. Several temperature sensors are installed in certain positions of the chamber to measure the temperature. By using Fluent software, a full-sized chamber model is developed. Meshing is a hybrid and is used as a boundary layer Mesh. The inlet and outlet temperature of the chamber and the air output rates, as the boundary conditions, are used in the simulation. Numerical analysis for K-ε and K-ω turbulence models is performed, and different wall conditions are investigated. The numerical simulation results are in good agreement with the measurement results. K-ε turbulence model with a scalable wall function provides better accuracy than other models. Changes in velocity and temperature are presented in graphs and contours at different positions of the compartment.

1. Introduction

Today, attention to indoor air conditioning is becoming increasingly important. Ventilation systems are used under safe and high-quality conditions with minimal energy dissipation in order to provide the most favorable environmental conditions through the flow of air and prevention of contamination accumulation.

The shape of air flow in the interior is heavily influenced by the air distribution system and the way air enters and exits. In the simplest case, airflow can naturally flow into buildings, halls, tunnels, electricity chambers and other chambers such as computer cases. However, there will not be enough room for the airflow generated by the movement of objects inside these spaces.

Therefore, to improve indoor airflow and design of buildings, it is very important to explore the most efficient ventilation systems. While natural ventilation does not force the electric energy in exchange, mechanical ventilation requires a certain amount of energy to activate the fans and adjust the auto input and other electrical equipment. Obviously, energy efficiency optimization is needed to reduce the demand for electric power and also reduce costs. Optimizing building design and improving ventilation efficiency may help reduce costs and indirectly reduce fossil fuel consumption or other non-renewable resources and also may help control global warming.

2. Literature review

Two methods for analyzing indoor environment problems are used: direct measurement by electronic instrumentation and computational fluid dynamics (CFD). The CFD method is a very necessary technique in many fields of science and engineering [1-3]. However, a proper instrumentation system is required to validate simulation [4]. The use of CFD techniques to solve complex fluid problems has greatly increased in recent years (Lee et al. 2007 [5] and Seo et al. [6]). CFD can also save the cost, time, and effort associated with the field experiments to establish the optimum system (Lee et al. [7]) but the accuracy needs to be assessed. There are several possibilities that can be studied through CFD simulations, such as airflow inside buildings as related to the ventilation system (Bartzanas et al., [8]; Blanes-Vidal et al., [9]; Seo et al., [10]; Saraz et al., [11]; Bustamante, [12]; Rong et al., [13]). Also, the choice of the proper turbulence model is one of the most important aspects in CFD modelling. Several studies have focused on the effect of various turbulence models on the final numerical solution, (Mistriotis et al., [14]; Gerdes et al., [15]; Sapounas et al., [16]; Garcia Sagrado et al., [17]; (Bartzanas et al., [18]; Stavrakakis et al., [19] ;). Li et al. [20] studied the vertical temperature profiles in rooms ventilated by displacement (full-scale measurement and nodal modeling). Merci et al. [21] experimentally studied the natural roof ventilation in full-scale enclosure fire tests in a small compartment. The impact of the different parameters was examined on the smoke layer depth and temperature variations in the vertical direction in the compartment. Lim et al. [22] conducted a numerical study on the characteristics of flow field, temperature and concentration distribution according to changing the shape of the separation plate of a kitchen hood system. Rees et al. [23] studied airflow and temperature distribution in a room with displacement ventilation and a chilled ceiling. Kang et al. [24] studied the improvement of natural ventilation in a large factory building using a louver ventilator. Dalley et al. [25] studied an Investigation of the Aerodynamic and Ventilation Characteristics of Poultry Transport Vehicles. Kacira et al. [26] used the commercial CFD program Fluent V4 to predict ventilation for different configurations of inlets and outlets in a greenhouse. Blanes-Vidal et al. [9] studied the application of computational fluid dynamics to predict the airflow in a mechanically ventilated commercial poultry building. Bustamante et al. [27] exploring ventilation efficiency in poultry buildings: the validation of computational fluid dynamics (CFD) in a cross-mechanically ventilated broiler farm. Statsenko et al. [28], they studied the temperature and velocity conditions of air flow in vertical channel of hinged ventilated facade of a multistory building. Christopher Y. Chao et al. [29], they studied the numerical and experimental study of velocity and temperature characteristics in a ventilated enclosure with underfloor ventilation systems. Gilkeson et al. [30] studied the quantifying passive ventilation within small livestock trailers using computational fluid dynamics. Roberto et al. [31], they studied the simulation of ventilation systems in a protected environment using computational fluid dynamics. Rodrigues et al. [32] studied the application of computational fluid dynamics on a study in swine facilities with mechanical ventilation system.
In all of the work done, items like the thermal layering of the air or air temperature distribution have been studied in laminar or turbulent flow.

3. Goal setting

The purposes of this study are to construct a compartment and develop different laboratory conditions and then validate the airborne CFD results with direct measurement. It also compares the results of turbulence models and eventually check the current in the enclosure. In addition to the thermal layering of the air and the distribution of air temperature, the distribution of air velocity and the presence of air awhirl flow as well as the absence of airflow, that causes the accumulation of air pollution in the closed space, are investigated.

4. Governing equation

The main idea in all CFD techniques is to analyze a set of partial differential equations (PDEs).

Continuity equation is:

$$\frac{\partial u}{\partial x_i}(\rho u_i) = 0 \tag{1}$$

Momentum equation is:

$$\frac{\partial u}{\partial x_j}(\rho u_i u_j) = -\frac{\partial p}{\partial x_i} + \frac{\partial \tau_{ij}}{\partial x_i} + S_u \tag{2}$$

In the high Reynolds numbers, the kinetic energy dissipation rate ε is equal to the viscosity coefficient by oscillating displacement. A precise transfer equation for fluctuating displacement, and thus loss rate, can be derived from the Navier Stokes equation.
The K-ε model contains the turbulent energy equation as:

$$\frac{\partial u}{\partial x_j}(\rho u_j k) = \frac{\partial p}{\partial x_i}\left(\mu + \frac{\mu_t}{\sigma_k}\right)\frac{\partial T}{\partial x_j} + \mu_t G$$
$$- \rho\varepsilon \tag{3}$$

and the loss rate equation is:

$$\frac{\partial u}{\partial x_j}(\rho u_j \varepsilon) = \frac{\partial}{\partial x_j}\left(\mu + \frac{\mu_t}{\sigma_\varepsilon}\right)\frac{\partial \varepsilon}{\partial x_j}$$
$$+ \frac{\varepsilon}{k}(C_1 \mu_t G - C_2 \rho\varepsilon) \tag{4}$$

The energy equation is as follows:

$$\frac{\partial(\rho u_j T)}{\partial x_j} = \frac{\partial}{\partial x_j}\left(\frac{\mu}{Pr} + \frac{\mu_t}{Pr_t}\right)\frac{\partial T}{\partial x_i}$$
$$+ S_T \tag{5}$$

where

$$\mu_t = C_\mu \frac{\rho k^2}{\varepsilon} \tag{6}$$

$$\tau_{ij} = -(\mu + \mu_t)\left(\frac{\partial u_i}{\partial x_j} + \frac{\partial u_j}{\partial x_i}\right) \tag{7}$$

$$S_u = -\frac{2}{3}(\mu + \mu_t)\frac{\partial}{\partial x_i}\left(\frac{\partial u_i}{\partial x_i}\right) \tag{8}$$

$$\mu_t G = -\left(\frac{\partial u_i}{\partial x_j} + \frac{\partial u_i}{\partial x_i}\right)\frac{\partial u_i}{\partial x_j}$$
$$-\frac{2}{3}\left(\rho k + \frac{\partial u_i}{\partial x_i}\right)\frac{\partial u_i}{\partial x_j} \tag{9}$$

In the above equations ρ is the density of the fluid (kg.m^{-3}); t is the time (s); x, x_i, and x_j are the components of length (m); u_i and u_j are the speed component (m.s^{-1}); P is the pressure (Pa); T_{ij} is the stress tensor (Pa); G is the gravitational acceleration (m.s^{-2}); C is the specific heat (W.kg^{-1}.k^{-1}); T is the temperature (°k); K is the thermal conductivity (Wm^{-1}.K^{-1}); and S_T is the heat source (W.m^{-3}).
The employed turbulent constant values of the standard turbulent model are shown in Table 1.

Table 1. Turbulent constants for K-ε standard model.

Constant	Value
C_1	1.44
C_2	1.92
C_μ	0.09
k	1
ε	0.9

5. Constructing the chamber

The study starts with the evaluation of ventilation systems and other constructed chambers (Fig. 1). The property and general capabilities of the system are then determined through consulting with experts in the field. The

main compartment, used for the diffusion and emission of the heat, is made of plexiglas. This chamber is in the shape of a rectangular cube with the dimensions of $16.1 \times 26.2 \times 48.6$ cm³, corresponding to height, width, and length, respectively. The thickness of the plate is 0.2 cm. A circular hole with a diameter of 5 cm is made at the end of the chamber to enable the installation of the exhaust fan. The hole locates in the middle of the enclosure. On the front wall, there are three rectangular entries of 2×3.2 cm², two of which are at a height of 10.5 cm and the other at 5 cm, for the air inlet.
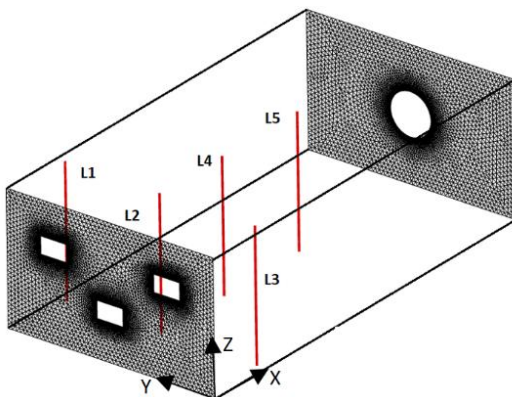
Fig. 1. Chamber geometry.

Then, the electric fans are installed in the place; afterward, all the walls are covered inside with a 6 mm thick elastomeric insulation. The density and heat transfer coefficient of this insulation range from 120 to 50 kg.m⁻³ and 0.032 to 0.036 W.m⁻¹.°k⁻¹, respectively; as a result, the amount of energy dissipation prevention is 85 to 90 percent. Electronic circuit maps are designed by software Proteus 8.1. Eventually, by using the CSS 5,012 software, the instructions for the microcontroller are written in language C, and after executing the commands in Proteus 8.1 software, the necessary electronic circuit tests are performed. In the next step, using the software and hardware of the PIC programmer, the commands are given to the microcontroller (PIC).The processor set (controller) is responsible for receiving commands and executing them by operators, receiving sensor information and sending information to the display. This series includes multi-fan, variable

temperature sensors, six keys, a PIC 16F877A microcontroller, and a display that is responsible for displaying the temperature of different points and fan speeds. The temperature sensors are carefully selected and placed according to the manufacturer's information (Datasheet) in the electronic circuit (Fig. 2). The temperature sensor (DS18B20, a digital one) is used to report the temperature accurately at any moment.
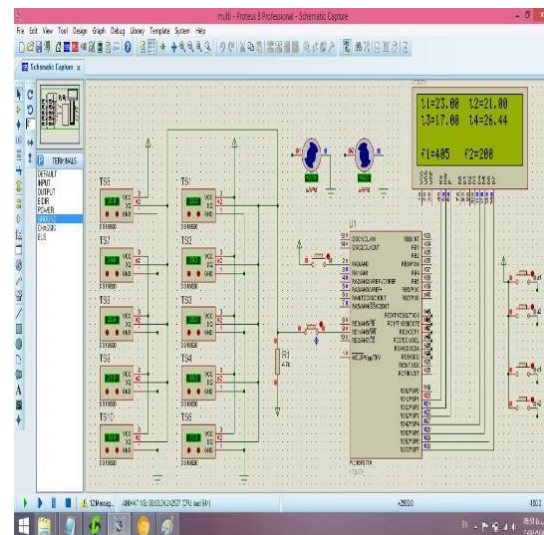

Fig. 2. Temperature sensors placement according to the datasheet.

The exact function of the sensor is within the range between a negative value of 55°C and a positive value of 125°C with a very high accuracy of about 0.0625°C with a quick reaction to the smallest temperature variations. The temperature conversion time is to a digital expression of 200 milliseconds and the maximum conversion and response time of 750 milliseconds. It should be noted that the total number of the sensors in this circuit is 22, which are placed in 3 categories. The position of the sensors inside this chamber is given in Table 1.

6. Performing the experiment

The test room air conditions have the following characteristics:
Air temperature at the outside of this chamber is 24.8 °C, the air velocity around the compartment is 0 m.s⁻¹, the air density at this

temperature is 1.184 kg.m^{-3}, and the dynamic viscosity is 1.97×10^{-10}.

An exhaust fan is located in the middle of the active part and middle inlet (inlet of the heater); the air is heated with a heater and from two other entrances, the air is sucked into the room. The sensors are located at two main positions; one group is used to determine the air temperature near the floor of the compartment at a height of 0.6 meters, and the other group is located at different altitudes to determine the temperature variation of the air (thermal layering) in the compartment. The remaining sensors includ 6 sensors in the inputs, 3 sensors in the outlets, 2 sensors on the outer wall of the enclosure, and a sensor in the vicinity of the open air outside the compartment. Fig. 3 shows position of the sensors inside the enclosure under the experimental conditions.

Table 1. The position of the sensors.

Sensor number	X, cm	Y, cm	Z, cm
1	18	1	0.6
2	18	12.8	0.6
3	18	24.5	0.6
4	42	1	0.6
5	42	12.8	0.6
6	42	24.5	0.6
7	18	12.8	3.5
8	18	12.8	7.75
9	18	12.8	12
10	18	12.8	14.8

Fig. 3. Location of sensors.

The velocity and temperature of the exhaust air are measured using a Vane speedometer with a precision of 0.1 m.s^{-1} and a thermometer, attached to it, with a precision of 0.1 °C at room temperature. In the incoming air condition unit, the average temperature of the inlet air, after

warmed by the heater, in scenario A is 39.33 °C. In scenario B, the average temperature is 45.12 °C while the mean temperature in the other two inputs is 25.28 °C. The air intake is based on fan suction. In the output air condition unit (the exhaust fan), the average outlet air temperature in scenario A is 28.94 °C, whereas, in scenario B, it is 35.82 °C and the mean air velocity is 1.5m.s^{-1} while the fan pressure is zero. Using the equation m=ρAV, the m_A and m_B, the mass flow rates of the exhaust fan are:

$$m_A = 1.1686 \times (\pi(2.5/100)^2) \times 1.5 = 0.0034418 \text{ kg.s}^{-1}$$
$$m_B = 1.1426 \times (\pi(2.5/100)^2) \times 1.5 = 0.0033652 \text{ kg.s}^{-1}$$

At this stage, an experimental study is conducted on a chamber that has mechanical longitudinal ventilation. This model has many applications in designing industrial and non-industrial ventilation systems. The enclosure is evaluated using a multisensory system. In this way, information about the air inside the compartment and properties such as temperature are gathered using sensors which are able to measure physical properties. Fig. 4 shows an overview of the built-in compartment set during testing. Then, numerical simulation of these two experiments is carried out and evaluated using the results of the experiments in the conditions of three inputs and one outlet (fan) on this compartment in terms of thermal imprinting as well as the temperature distribution at a specific height of the enclosure. In the end, the results are compared with each other.

Due to the position of the sensors, the temperature distribution is evaluated in two scenarios, each in two stages. One scenario is set with a height of 0.6 cm on the compartment surface while the other is set in a vertical mode. Proper distribution of the temperature produced by thermal sources such as heating and electronic equipment at a specific height of the internal surfaces is a common requirement for mandatory ventilation. The air temperature obtained at this height is according to the position of the sensors in the chamber. Table 2 shows the air temperature at a height of 0.6 cm

in scenarios A and B in the compartment. In these conditions, according to Tables 2 and 3, the average air temperature, which is mathematically obtained at the height of 0.6 cm, is 29.41±0.4 °C in scenario A (± standard deviation) and 30.93±0.49 °C in scenario B.
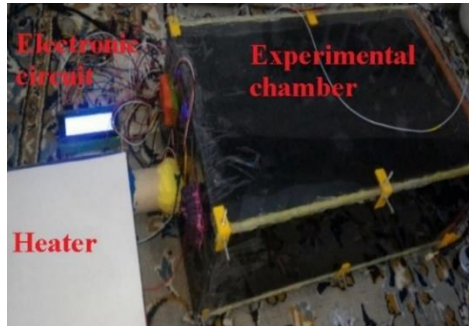

Fig. 4. Experimental chamber testing.

Table 2. Air temperature at the 0.6 cm height in scenarios A and B.

	Temperature in scenario A	Temperature in scenario B
1	29.12	30.42
2	30.24	31.84
3	29.12	30.36
4	29.24	30.9
5	29.6	31.18
6	29.18	30.9
Total absolute	176.5	185.6
Average	29.416	30.933
Standard deviation	0.403	0.496

Table 3. The main settings in the CFD simulations.

(I) The fixed settings and calculations
Three-dimensional (3D) double precision; Segregated; steady;
Turbulent model: the K-ε standard or the K-ω SST model;
Wall behavior: wall functions for the K-ε standard model: Scalable wall functions;
For the solution of the algorithm, the followings are solved:
Pressure and speed; the SIMPLE algorithm;
Pressure discriminant design; standard
Momentum: second order upwind;
Kinetic energy turbulence; second order upwind;
Turbulence loss rate; second order upwind;
Energy; second order upwind;
Gravitational acceleration: (m s^{-2}) 9.81;
Atmospheric pressure: (Pa) 101325

The information related to the average temperature of air at a certain height from the interior surfaces helps us to choose the right conditions to reach optimal temperatures. The temperature of the layer produced by thermal

sources at the internal surfaces is a common feature of floating ventilation called displacement ventilation. In industry and the interior, thermal layering and vertical temperature difference between the ceiling and floor are essential for the design and assessment of displacement ventilation. The temperature of the air obtained on a vertical line at different heights is due to the thermal layering in the enclosure. In Fig. 5, the air temperature obtained in the experimental method with x=18 cm and y=12.8 cm and with specific heights are shown in the two scenarios A and B.
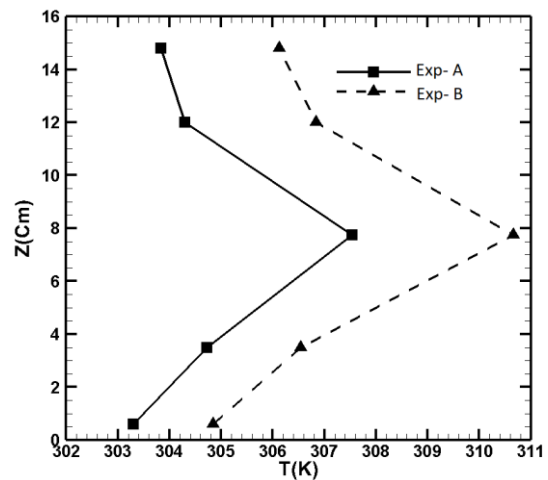

Fig. 5. The measured value of the temperature at x=18 cm and y=12.8 cm with different altitudes for the scenarios A and B.

The temperature changes for the two scenarios are similar. At the bottom of the chamber, there is the lowest temperature at the maximum height, and the temperature increases with increasing the height to the upper part of the chamber, and the temperature again decreases. At all heights, the temperature of scenario B is greater than that of scenario A.

7. Numerical simulation

The computational fluid dynamics method is used in the simulations. The Fluent software is used to realize all the simulations. The design of the test chamber model is done in the ANSYS Design Modeler software. Boundary layer mesh is developed in the Meshing software in the inflation section. The lowest boundary mesh

distance from the center point of the adjacent cell wall is to the wall of different surfaces of 0.005 mm and with the growth of 1.25. There are 11 cells in this area (Fig. 6). An unstructured tetrahedral mesh is used for parts of this simulation. As a result, triangular elements are used for the surface mesh, and prism/wedge elements are used for the lowest boundary mesh. The surface grids on the walls, fans, and entrances are produced in facial sizes; thus, the mesh density is higher near these faces than farther away. The boundary conditions are applied as the pressure inlet for the inlet, the exhaust fan for the outlet, and other settings according to the parameters given in Table 3. The test of this chamber with longitudinal ventilation is carried out under the environmental conditions given in Table 4. The results are fully converged after 7000 iterations.
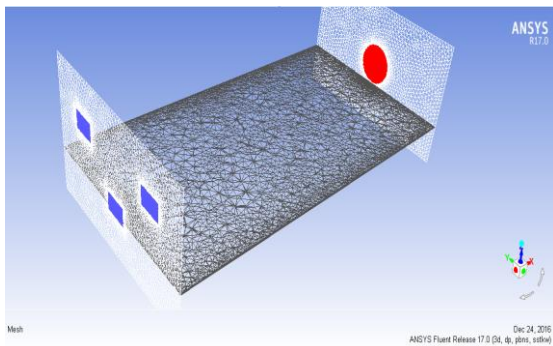
Fig. 6. Production of link mesh in the flow field.

In order to investigate the convergence of the numerical solution, the temperature and velocity variations in several points are plotted according to the repetition, which remains constant after about 7000 repetitions to the third digit of the decimal value of the temperature and velocity constant. The simulation is performed for the two models of K-ε standard and K-ω SST. Fig. 7 shows the contour y^+ on the walls of the chamber for a state analyzed by the K-ε disturbance model. The maximum value of y^+ is about 5, which covers only very small areas of the wall.

The value of y^+ in the major part of the wall is less than 3. For the K-ω disturbance model, with respect to the finiteness of the boundary layer

network, the value of y^+ on all the walls is less than 1. The simulation result values are compared with the experimental data for the average temperature of the specific points as well as the vertical line temperature specified in the enclosure. In Table 5, the temperature values and percentage error rates are given between the simulation results and the experimental data at a height of 0.6 cm.

Table 4. Environmental conditions

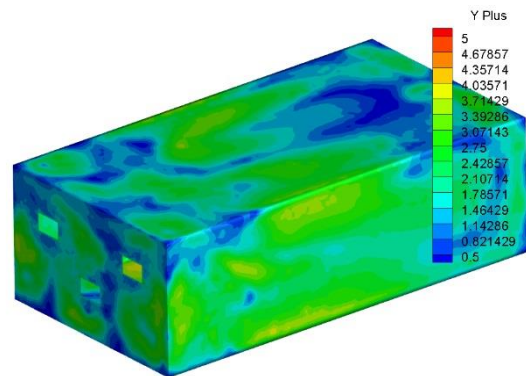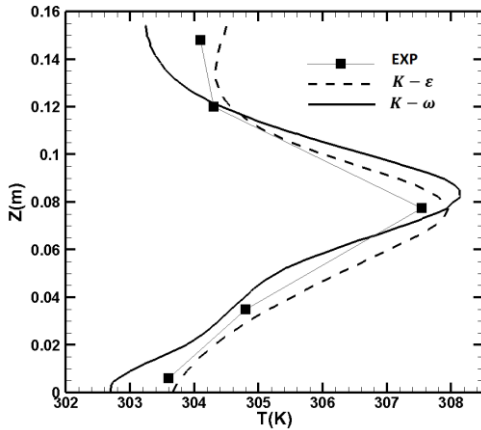| (II) The boundary conditions		
Output (fan):		
Pressure (ms^{-1})	0	
Mass flow rate (kgs^{-1})	0.0034418 (A)	0.0033652(B)
Air temperature (°C)	28.94 (A)	35.82 (B)
Room air intake:		
Air pressure (ms^{-1})	0	
Air temperature (°C)	25.28	
Inlet of hot air:		
Air pressure (ms^{-1})	0	
Air temperature (°C)	39.33 (A)	45.12 (B)
Free air temperature (°C)	24.38	

Fig. 7. Contour of y^+ on the chamber walls.

For the models A and B, the precision of the K-ε model results is in very good agreement with those obtained from the measurement data, although the error value for the K-ω model is about 6.5% and 4.53% for the scenarios A and B, respectively. For the scenarios A and B, the simulation results are presented in Figs. 8 and 9 using the two models of the turbulence K-ε and K-ω, respectively.

Table 5. The simulation results and the experimental data of temperature (°C) (Standard deviation ± mean).

Scenario	Height	Method	Model		Mean	Standard deviation	Error
A	0.6	EXP	-	-	29.416	±0.40 (6)	
		CFD	K-ε	Standard-scalable wall function	29.387	±0.60 (6)	0.098
			K-ω	SST	27.52	±0.47 (6)	6.5
B	0.6	EXP	-	-	30.933	±0.49 (6)	
		CFD	K-ε	Standard-scalable wall function	30.888	±0.69 (6)	0.145
			K-ω	SST	29.531	±0.54 (6)	4.53

The process of temperature changes along the vertical line is the same for the two disturbance models and in accordance with the experimental results. In Fig. 8, the temperature at the bottom of the chamber is about 32 °C, which, with an increase in height, reaches a maximum value of 38 °C at mid-height and decreases to 34 in the roof of the chamber. In the middle section of the chamber height, there is a very good match between the two disturbance models and the measurement results.

changes along the vertical line in Fig. 9 is similar to the previous one. The difference between these two scenarios is in the temperature range in different places. In this case, the results of the K-ε disturbance model are better than those of the K-ω model obtained through laboratory data.

For further investigation of the K-ε and K-ω disturbances, in Fig. 10, the temperature distribution of the perpendicular plate passing through the heater is presented for scenario A.

Fig. 8. Temperature variation in height for the position x=18 cm and y=12.8 cm for scenario A.
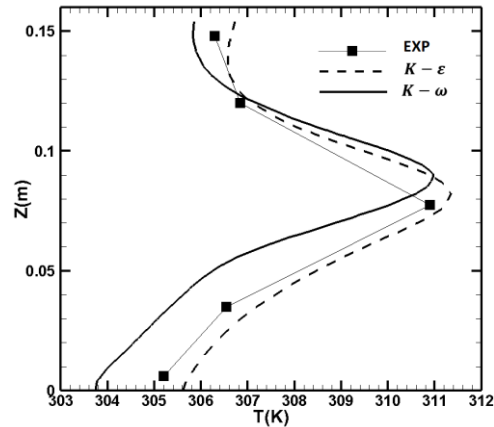
Fig. 9. Temperature variations in height for the position x=18 cm and y=12.8 cm for scenario B.

However, in the lower elevation near the floor and at high altitudes near the ceiling of the hall, the differences between the numerical results are apparent. The results obtained by using the K-ω disturbance model near the wall has a significant difference. In the bottom wall, the temperature difference is about 0.1%, and in the upper wall, the temperature difference for the K-ε disturbance model is at the most percent. For scenario B, the diagram of temperature

When the hot air enters the chamber, it moves toward its roof. In Fig. 3, there are differences in the temperature distribution. In the turbulent model, the temperature distribution of the K-ε occurs more frequently (Fig. 10(a)). If the temperature distribution of the K-ω model is more than the longitudinal influence of the temperature, the lateral surfaces and corners will be less affected by the inlet temperature (Fig. 10(b)).
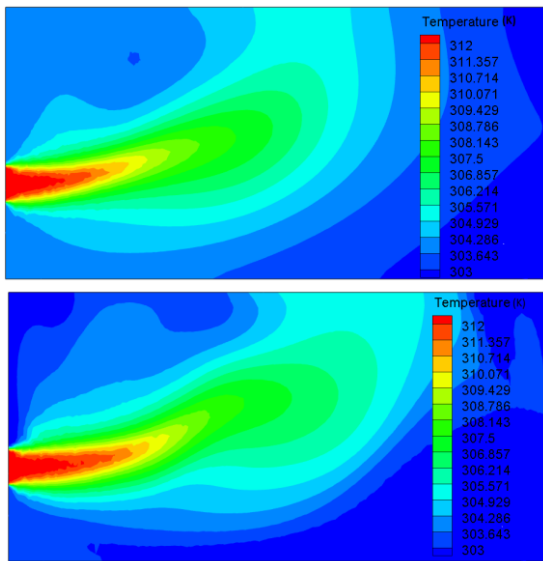
Fig. 10. Distribution of static temperature in the middle section of the chamber passing through the heater for scenario A; (a) K-ε and (b) K-ω.

Fig. 11 shows the velocity distribution in X-axis direction along with the streamlines. For both models, the maximum speed of 1.6 and the minimum speed of -0.2 are the same, and also the flow through the heater into the compartment is leaked due to the high flow rate of the flow lines upward and the air at the outlet by the fan sucked and driven out. With more accuracy on the streamlines and the comparison between the two turbulence models, the difference between the two models is noticed. In the turbulence model K-ε, after flowing into the enclosure and reducing the flow energy, two vortices are formed around the input current (Fig. 11(a)). In the turbulence model K-ω , as shown in Fig. 11(b), only one vortex is formed in the middle of the enclosure. Flow direction is the top of the vortex to the outlet, while Flow direction, the vortex bottom, returns to the inlet of the compartment.

Fig. 12 shows the variations of component x of the speed along the three lines of L2, L4, and L5 According to the graphs in Fig. 12, the maximum speed is near the wind speed heater, and the amount of speed variation is also higher for this position (line L2). Therefore, the signal of a negative velocity is near the bottom of the compartment, that is, the flow returned to the heater, and in the close range of the ceiling, the speed is almost zero. (as shown in Fig. 1) for

scenario A simulated using the K-ε turbulence model.

As the distance from the heater increases (line L4), the velocity reduces by a maximum and the distance increases to the ceiling.
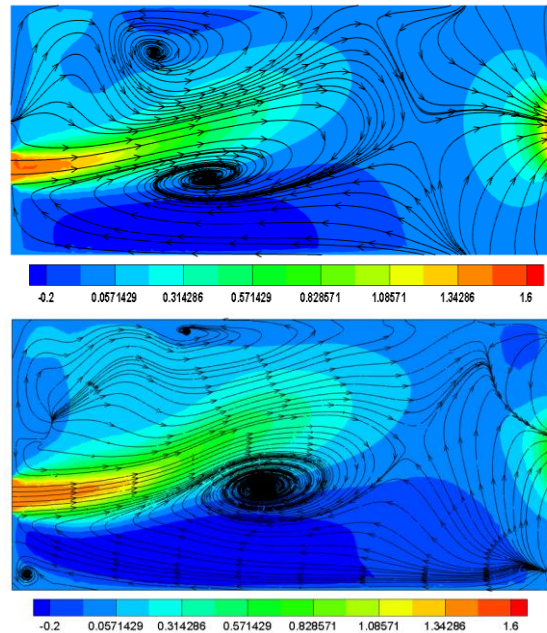

Fig. 11. Distribution of the component x; the speed and streamlines on the middle of the chamber passing through the heater for scenario A; (a) K-ε and (b) K-ω.
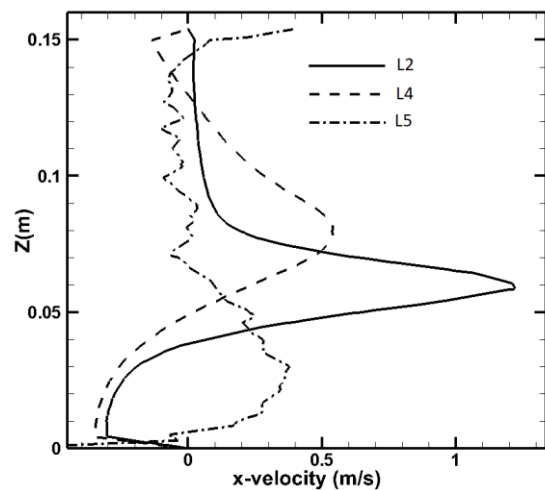

Fig. 12. Oscillation of the component x speed along the vertical line of the three lines of L2, L4, and L5 using the K-ε model for scenario A.

In this case, the speed symbol near the floor of the chamber is negative. The variation in speed is similar to that of the line L5, which i close to the output of the chamber. The speed signal, near the floor, is positive and the altitudes are higher than the speed of about zero.

Fig. 13 shows the temperature changes corresponding to Fig. 12. The temperature changes for the three specified lines are the same as the speed changes. This study shows that in the compartment, according to the input and output layout, there are variations in temperature where it can be compared to the simulation model for the two disturbance models.

Figs. 14 and 15 respectively show the velocity and temperature distribution along the line L2 for the two turbulence models K-ε and K-ω. The line L2 is in the middle of the compartment and in the vicinity of the heater, as shown in the Fig.14 and 15.

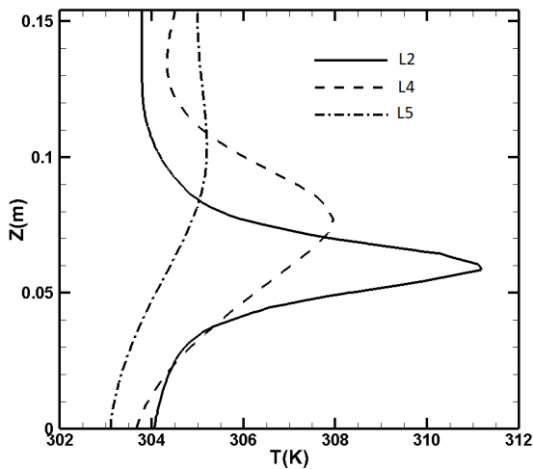**Fig. 13**. Static temperature variation along the vertical line of the three lines of L2, L4, L5 using the K-ε model for scenario A.

For this line, the process of variations in speed and temperature is similar for the two models of turbulence, but the difference between the results is clear in vicinity of the container chamber. For further reviewing, the results are compared along line L3. Fig. 16 shows the velocity distribution of this state. Due to the shortage of speed variations along this line, the difference between the results of two more disturbing models is clear
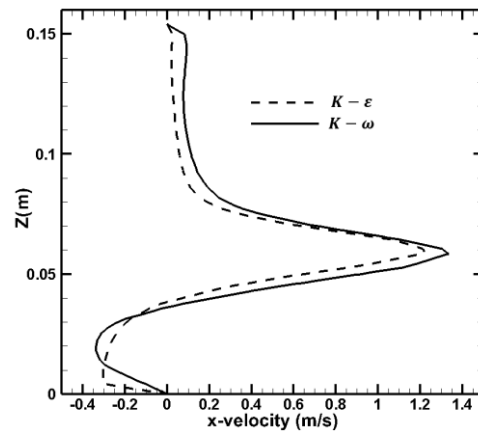

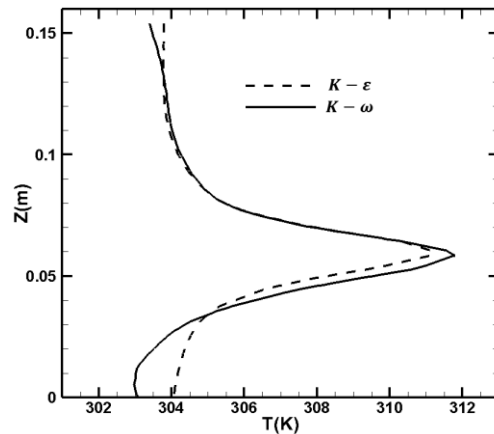**Fig. 14.** Changes in the velocity component x along line L2.

Fig. 15. Static temperature changes along line L2.

Changes in the static temperature associated with the line L3 in Fig. 17 show the difference between the results of the two models of turbulence. The temperature obtained from the K-ε method is almost constant along this line.
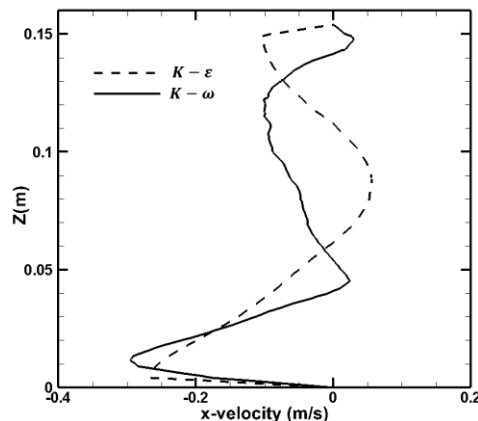

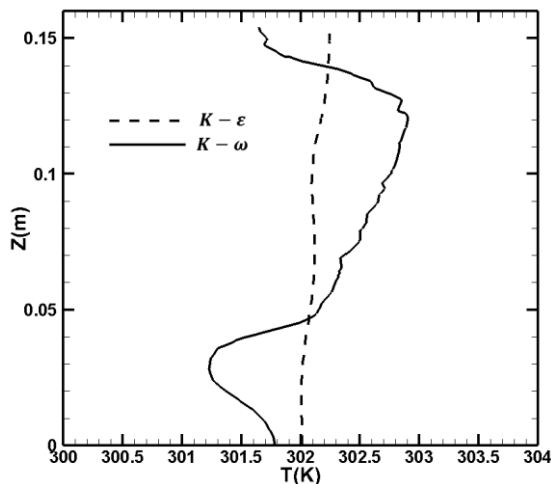**Fig. 16.** Changes in the velocity component x along line L3.

Fig. 17. Static temperature changes along line L3.

8. Conclusions

In this paper, a chamber with a specific dimension is developed to form a temperature and velocity distribution of three inputs and one output. The air, from the middle inlet, is heated by a heater and dumped by a fan. By installing temperature sensors at the inlet, outlet and certain points of the enclosure, the temperature of these points is measured with high precision. To test the K-ε and K-ω turbulent models in a correct simulation of the temperature and velocity distribution, the experimental model is simulated using the Fluent software. The comparison of the average measured temperature of the sensors with the corresponding values in the numerical simulation shows that the K-ε turbulent model has an error rate less than 1%; however, the error rate is about 6% for the K-ω model. Comparison of temperature variations between the two disturbance models and measured results confirms this. The error rate of about 6% is surely acceptable by the numerical method. The difference between the two models of turbulence is determined by the prediction of flow pattern and the location of vortex formation, which, in some cases, yields completely different results. This is due to the fact that there is a good match between the results of the turbulence model K-ε and the measurement data in terms of average

temperature and temperature variations along a given line.

References

[1] E. Lee, C. Feigly, and J. Khan, "An investigation of air inlet velocity in simulating the dispersion of indoor contaminants via computational fluid dynamics", *Annals Occupational Hygiene*, Vol. 46, No. 8, pp. 701-712, (2002).

[2] L. Yuguo, and A. Delsante, "Derivation of capture efficiency of kitchen range hoods in a confined space", *Building in Environment*, Vol. 31, No. 5, pp. 461-468, (1996).

[3] U. Madsen, N.O. Breum, and P.V. Nielsen, "Local exhaust ventilation-a numerical and experimental study of capture efficiency", *Building and Environment*, Vol. 29, No. 3, pp. 319-323, (1994).

[4] E. Bustamante, E. Guijarro, F.J. García-Diego, S. Balasch, A.G. Torres, "Multi sensor system for isotemporal measurements to assess indoor climatic conditions", *poultry farms Journal-sensors*, Vol. 12, No. 5, pp. 5752-5774, (2012).

[5] I. Lee, S. Sase, and S. Sung, "Evaluation of CFD accuracy for the ventilation study of a naturally ventilated broiler house". *Japan Agricultural Research Quarterly*, Vol. 41, No. 1, pp. 53-64, (2007).

[6] I. Seo, I. Lee, O. K. Moon, H. T. Kim, H. S. Hwang, and S. Hong, "Improvement of the ventilation system of a naturally ventilated broiler house in the cold season using computational simulations". *Biosystems Engineering*, Vol. 104, No. 1, pp. 106-117, (2009).

[7] I. Lee, S. Sase, H. Han, H. Hong, "Ventilation design for a chick incubator using computational fluid dynamics". *Japan Agricultural Research Quarterly*, Vol. 43, No. 3, pp. 227-237, (2009).

[8] T. Bartzanas, C. Kittas, A. A. Sapounas, C. H. Nikita-Martzopoulou, "Analysis of airflow through experimental rural buildings: sensitivity to turbulence models". *Biosystems Engineering*, Vol. 97, No. 2, pp. 229-239, (2007).

[9] V. G. Blanes-Vidal, S. Balasch, A. G. Torres, "Application of computational fluid dynamics to the prediction of airflow in a mechanically ventilated commercial poultry building", *Biosystems Engineering*, Vol. 100, No. 1, pp. 105-116, (2008).

[10] I. Seo, I. Lee, O. Moon, S. Honga, H. Hwanga, j. P. Bitog, K. Kwona and Z. Yec, "Modelling of internal environmental conditions in a full-scale commercial pig house containing animals", *Biosystems Engineering*, Vol. 111, No. 1, pp. 91-106, (2012).

[11] J. A. Saraz, M. A. Martins, K. S. Rocha, N. S. Machado, and H. J. Velasques, "Use of computational fluid dynamics to simulate temperature distribution in broiler houses with negative and positive tunnel type ventilation systems". *Actualidad & Divulgacion Cientifica,* Vol. 16, No. 1, pp. 159-166, (2013).

[12] E. Bustamante, F. Garcia-Diego, S. Calvet, F. Estelles, P. Beltran, and A. Hospitaller, "Exploring ventilation efficiency in poultry buildings: the validation of computational fluid dynamics (CFD) in a cross-mechanically ventilated broiler farm". *Energies*, Vol. 6, No. 5, pp. 2605-2623, (2013).

[13] L. Rong, P. V. Nielsen, B. Bjerg, and G. Zhang, "Summary of best guidelines and validation of CFD modeling in livestock buildings to ensure prediction quality". *Computers and Electronics in Agriculture,* Vol. 121, No. 1, pp. 180-190, (2016).

[14] Y. Li, M. Sandberg, and L. Fuchs, "Vertical temperature profiles in rooms ventilated by displacement: full -scale measurement and nodal modelling". *Indoor Air*, Vol. 2, No. 4, pp. 225-243, (1992).

[15] B. Merci, P. Vandevelde, "Experimental study of natural roof ventilation in full-scale enclosure fire tests in a small compartment". *Fire Safety Journal*, Vol. 42, No. 8, pp. 523-535, (2007).

[16] K. Lim, and C. Lee, "A numerical study on the characteristics of flow field,

temperature and concentration distribution according to changing the shape of separation plate of kitchen hood system", *Energy and Buildings*, Vol. 40, No. 2, pp. 175-184, (2008).

[17] J. Simon, and P. Haves, "An experimental study of air flow and temperature distribution in a room with displacement ventilation and a chilled ceiling", *Building and Environment,* Vol. 59, No. 1, pp. 358-368, (2013).

[18] J. H. Kang, and S. J. Lee, "Improvement of natural ventilation in a large factory building using a louver ventilator", *Building and Environment,* Vol. 43, No. 12, pp. 2132-2141, (2008).

[19] S. Dalley, C. Baker, X. Yang, P. Kettlewell, and R. Hoxey, "An Investigation of the Aerodynamic and Ventilation Characteristics of Poultry Transport Vehicles: Part 3, Internal Flow Field Calculations, *Journal of Agricultural Engineering Research,* Vol. 65, No. 2, pp. 115-127, (1996).

[20] M. Kacira, T. Short, and R. Stowell, "A Cfd Evaluation of Naturally Ventilated, Multi-Span, Sawtooth Greenhouses". *Contribution to journal › Article*, Vol. 41, No. 3, pp. 833-836, (1998).

[21] E. Bustamante, F. Garcia-Diego, S. Calvet, F. Estelles, P. Beltran, and A. Hospitaller, "Exploring ventilation efficiency in poultry buildings: the validation of computational fluid dynamics (CFD) in a cross-mechanically ventilated broiler farm", *Energies,* Vol. 6, No. 5, pp. 2605-2623, (2013).

[22] A. Mistriotis, G. P. A. Bot, P. Picuno and G. Scarascia-Mugnozza, "Analysis of the efficiency of greenhouse ventilation using computational fluid dynamics". *Agricultural and Forest Meteorology*, Vol. 85, No. 3-4, pp. 217-228, (1997).

[23] F. Gerdes, and D. Olivari, "Analysis of pollutant dispersion in an urban street canyon". *Journal of Wind Engineering and Industrial Aerodynamics*, Vol. 82, No. 1-3, pp. 105-124, (1999).

[24] A. A. Sapounas, H. J. C. van Dooren and M. C. J. Smits, "Natural ventilation of

commercial dairy cow houses: simulating the effect of roof shape using CFD". *International Conference of Agricultural Engineering*. AGENG-2012, Valencia, Spain, (2012).

[25] A. P. Garcia Sagrado, J. van Beeck, P. Rambaud and D. Olivari, "Numerical and experimental modelling of pollutant dispersion in a street canyon". *Journal of Wind Engineering and Industrial Aerodynamics*, Vol. 90, No. 4-5, pp. 321-339, (2002).

[26] T. Bartzanas, C. Kittas, A. A. Sapounas and C. Nikita-Martzopoulou, "Analysis of airflow through experimental rural buildings: Sensitivity to turbulence models". *Biosystems Engineering*, Vol. 97, No. 2, pp. 229-239, (2007).

[27] G. M. Stavrakakis, M. K. Koukou, M. G. Vrachopoulos and N. C. Markatos, "Natural cross-ventilation in buildings: Building-scale experiments, numerical simulation and thermal comfort evaluation". *Energy and Buildings*, Vol. 40, No. 9, pp. 1666-1681, (2008).

[28] C. Gilkeson, H. Thompson, M. Wilson, and P. Gaskell, "Quantifying passive ventilation within small livestock trailers using Computational Fluid Dynamics". *Computers and Electronics in Agriculture*, Vol. 124, No. 1, pp. 84-99, (2016).

[29] C. Roberto, B. Ricardo, and G. Cristiane, "Simulation of ventilation systems in a protected environment using computational fluid dynamics", *Journal of the Brazilian Association of Agricultural Engineering,* Vol. 37, No. 3, pp. 414-425, (2017).

[30] V. Rodrigues, L. Sabino, and N. Roberto, *"*Application of computational fluid dynamics on a study in swine facilities with mechanical ventilation system", *Scientia Agricola,* Vol. 75, No. 3, pp. 173-183, (2018).

[31] E. Statsenko, A. Ostrovaia and A. Pigurin, "Temperature and velocity conditions of air flow in vertical channel of hinged ventilated facade of a multistory building", *E3S Web of Conferences*, Vol. 33, No. 7, pp. 02038 (2018).

[32] M. P. Wan, C. Y. Chao, "Numerical and experimental study of velocity and temperature characteristics in a ventilated enclosure with underfloor ventilation systems", *Indoor Air-black well publishing*, Vol. 15, No. 5, pp. 342-355 (2005).